Journal of Visualization, Vol. 4, No. 2 (2001) 139-150

Quantitative Visualization of the Leading-edge Vortices on a Delta Wing by Using Pressure-sensitive Paint

Egami, Y.*1, Iijima, Y.*1, Amao, Y.*1, Asai, K.*1,
Fuji, A.*2, Teduka, N.*2 and Kameda, M.*2

*1 National Aerospace Laboratory, 7-44-1 Jindaiji Higashimachi, Chofu, Tokyo 182-8522, Japan.
e-mail: yegami@nal.go.jp
*2 Tokyo University of Agriculture and Technology, 2-24-16 Naka-cho, Koganei, Tokyo 184-8588 Japan.

Received 7 August 2000.
Revised 17 January 2001.

***Abstract*:** Leading-edge vortices on a simple delta wing were visualized by using pressure-sensitive paint (PSP). PSP is an optical pressure measurement technique based on oxygen quenching of luminescent molecules. In the present study, we used PSP composed of platinum octaethylporphyrine (PtOEP) and fluoropolymer (poly-IBM-co-TFEM [Poly (isobutylmethacrtlate-co-trifluoroethylate)]). This new paint has higher sensitivity to pressure and lower sensitivity to temperature than previous ones, reducing an error due to temperature variation during a wind tunnel test. A thin coating of PSP was applied to a delta wing model with 70-degree leading-edge sweep. The coating was excited by Xenon light and emission from the coating was detected by a high-resolution CCD camera. Tests were done at subsonic speeds in the 0.2-m Supersonic Wind Tunnel at the National Aerospace Laboratory in Japan. Complicated flow structures on the delta wing including primary and secondary vortices were clearly visualized using pressure-sensitive paint. An *a priori* calibration technique was used to convert measured luminescent intensity into pressure. The obtained pressure distributions were in good agreement with pressure tap data. Pressure maps were obtained for various Mach numbers, Reynolds numbers and angles of attack. It was found that an increase in Mach number delayed vortex breakdown while Reynolds number had little effect on the vortex formation.

***Keywords*:** pressure-sensitive paint, image analysis, delta wing, leading-edge vortices, vortex breakdown.

1. Introduction

One of the most important requirements in a wind tunnel test is to measure surface pressure distribution on wind tunnel models. Usually, pressure taps and electric pressure scanners are used for measuring surface pressure. However, the number of pressure taps on a model is limited by space and cost, which makes it difficult to observe the flow field details over the entire model surface.

Recently, a new technique using pressure-sensitive paint (PSP) has been developed as an alternative for measuring surface pressure distributions. PSP is an optical surface measurement method based on a photochemical reaction known as oxygen quenching of luminescent molecules.

Using PSP, pressure distributions on aerodynamic surfaces can be acquired with high spatial resolution and troublesome model preparation is not required. Flow structures that have not been detected with discrete measurement of pressure taps can be visualized using PSP. In addition, PSP is regarded as a non-intrusive method since application of a thin paint coating does not disturb the flow around the model. It is also noted here that PSP is

not a qualitative visualization method. It is a quantitative measurement technique. So, we can use the PSP-derived data in designing aerodynamic vehicles and in validating analytical methods.

To ensure the accuracy of PSP, however, we have to correct temperature effects since the luminescent intensity from PSP coating depends both on pressure and temperature. PSP is usually composed of luminescent molecules and oxygen permeable binder. The characteristics of PSP are determined by the properties of these two components. Liu et al. (1999) have shown that oxygen diffusivity of the binder is the most important factor in determining temperature effects of PSP. In this context, it is desirable to use a polymer binder with lower diffusion barrier to oxygen. Amao et al. (1999) have synthesized a new fluoropolymer called poly(IBM-co-TFEM) [Poly (isobutylmethacrtlate-co-trifluoroethylate)]. The oxygen permeability of fluoropolymer will be large as an oxygen affinity is induced by the large electro negativity of fluorine. We adopted this new polymer as a binder of PSP based on platinum octaethylporphyrine (PtOEP). Results from static calibration tests have shown that PSP with fluoropolymer has much smaller temperature sensitivity than the one with conventional silicone binder like GP197.

This new PSP was applied to a delta wing model with 70° leading-edge sweep. Experiments were made at subsonic Mach numbers in the 0.2-m Supersonic Wind Tunnel at the National Aerospace Laboratory in Japan. The paint was excited by Xenon light and luminescent images were acquired using a 14bit CCD camera. The pressure distributions on the model were then reconstructed from obtained PSP intensity images. By comparing PSP-derived data with pressure tap data, the accuracy of PSP has been evaluated. From the images obtained at varying Mach number, Reynolds number and an angle of attack, the effects of these parameters on the leading-edge vortices on the delta wing were discussed in detail.

2. Photo-physical Foundations of Pressure-sensitive Paint

PSP is a technique based on oxygen quenching of luminescent molecules. The luminescent molecules like platinum porphyrine emit luminescence (fluorescence and/or phosphorescence) when they are irradiated by excitation light. The intensity of luminescence increases as oxygen concentration decreases, while the luminescent intensity decreases as oxygen concentration increases. This phenomenon is called oxygen quenching.

Theoretically, the luminescent intensity, I, is related to oxygen concentration, by the following Stern-Volmer equation.

$$\frac{I_0}{I} = 1 + K_{sv}(T)[\mathrm{O_2}] \tag{1}$$

where I_0 is the luminescent intensity when oxygen concentration is zero, T is temperature, K_{sv} is Stern-Volmer constant and $[O_2]$ is oxygen concentration.

According to Henry's law, the oxygen concentration in a paint layer is proportional to the partial pressure of oxygen in the air. For air, the partial oxygen pressure is 21% of air pressure. Then, the Stern-Volmer equation, Eq. (1), can be expressed in terms of air pressure, P, as

$$\frac{I_0}{I} = 1 + K_{sv}(T) \cdot S \cdot 0.21 \cdot P = 1 + K(T) \cdot P \tag{2}$$

where S is Henry's solubility constant and $K = 0.21SK_{sv}$.

For wind tunnel testing, Equation (2) is usually normalized by a luminescent intensity, I_{ref}, at a known constant reference pressure, P_{ref}, under wind-off condition. Thus, the Stern-Volmer relation can be put in a form suitable for aerodynamic testing purposes.

$$\frac{I_0}{I_{ref}} = 1 + K(T)P_{ref}, \quad \frac{I_0}{I} = 1 + K(\mathrm{T})\mathrm{P} \tag{3}$$

$$\frac{I_{ref}}{I} = A(T) + B(T) \cdot \left(\frac{P}{P_{ref}} \right) \tag{4}$$

where,

$$A(T) = \frac{1}{1 + K(T)P_{ref}} \quad \text{and} \quad B(T) = \frac{K(T)P_{ref}}{1 + K(T)P_{ref}}.$$

Note that a non-quenched intensity, I_0, in Eq. (2), has been eliminated in Eq. (4). Therefore, the effects of spatial non-uniformities of illumination, paint thickness and luminophore concentration can be eliminated by the rationing procedure.

A more general expression accounting of nonlinear effects is as follows.

$$\frac{I_{ref}}{I} = A(T) + B(T)\cdot\left(\frac{P}{P_{ref}}\right) + C(T)\cdot\left(\frac{P}{P_{ref}}\right)^2 + \cdots \tag{5}$$

The coefficients A, B and so on in this formula have to be determined by static calibration tests.

3. Static Calibration Tests of PSP

Calibration tests were conducted for three PSPs to evaluate the effects of binder materials. Table 1 shows the composition of each PSP. Platinum Octaethylporphyrin (PtOEP) is used as luminophore for these PSPs while three different kinds of polymer were used as binder.

Table 1. The composition of PSPs used in the present work.

	Luminophore	Binder	Polymer	Solvent
PSP-1	PtOEP (6.0mg)	Poly-IBM-co-TFEM	0.5mg	20.0m*l*
PSP-2	PtOEP (6.0mg)	Silicone polymer (GP197)	20.0ml	
PSP-3	PtOEP (6.0mg)	Poly-IBM	0.5mg	20.0m*l*

PSP-1 is a PSP using new fluoropolymer, Poly-IBM-co-TFEM, as binder. PSP-2 is a first-generation PSP using silicone polymer GP197 as binder. PSP-3 using Poly-IBM as binder was also tested to evaluate the effect of the fluorine group on PSP characteristics. Sample plates were prepared by applying these paints on aluminum plates using an airbrush.

A schematic of the PSP calibration chamber is shown in Fig. 1. Paint samples are installed in a pressure chamber where both pressure and temperature can be controlled. A 300-W Xenon arc lamp operated by a stable DC power supply is used as an excitation light source. The excitation light is delivered through a quartz optical guide to the samples under calibration. A 400±50 nm band-pass filter was placed at the tip of the optical guide.

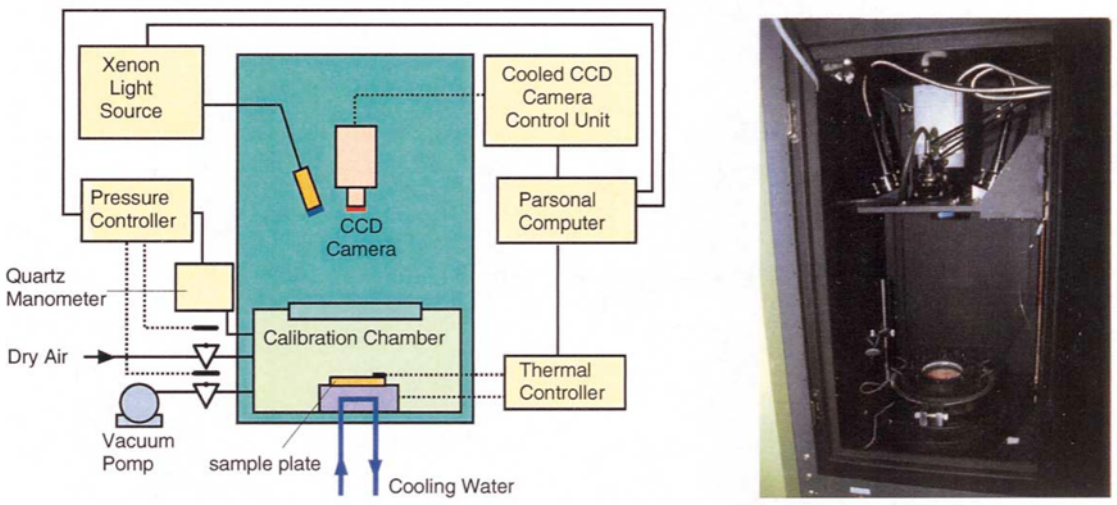

Fig. 1. Schematic sketch and a picture of the calibration chamber for PSP.

A scientific-grade cooled CCD digital camera was used for detecting emission from the sample. This camera has 1000×1018 pixel resolution and 14bit intensity resolution. To separate the paint emission from excitation light, a 650±20 nm band-pass filter is placed in front of the camera object lens. Calibration was done in the range of pressure from 5 to 100kPa and in the range of temperature from 283 to 333K.

The luminescent intensities of PSP-1, PSP-2 and PSP-3 are plotted in Fig. 2 as a function of pressure. The reference pressure is 100kPa and the reference temperature is 293.1K. For PSP-1 and PSP-3, the reciprocal of luminescent intensity ratio, I/I_{ref}, changes linearly with pressure ratio, P/P_{ref}. On the other hand, a calibration curve for PSP-2 (GP197 as binder) is slightly non-linear. It is noted that the calibration results strongly depend on temperature.

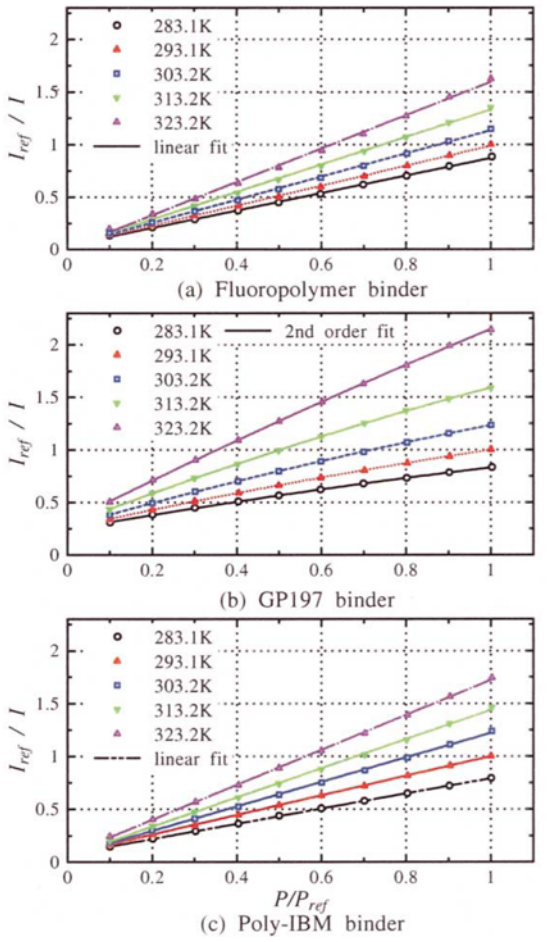

Fig. 2. Stern-Volmer plots for PSPs with different binders at several temperatures from 283.1K to 323.2K, where I_{ref} is the luminescent intensity at the reference pressure P_{ref} (100kPa) and 293.1K.

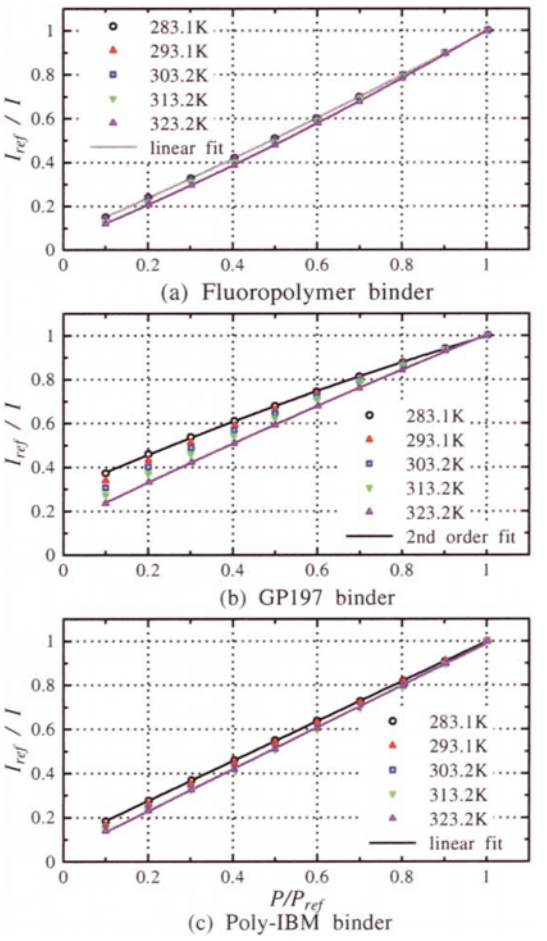

Fig. 3. Stern-Volmer plots for PSPs with different binders at several temperatures from 283.1K to 323.2K, where I_{ref} is the luminescent intensity at the reference pressure P_{ref} (100kPa) and each temperature.

Figure 3 shows the same data as in Fig. 2 plotted in Stern-Volmer form using the intensity at P_{ref}=100kPa for each temperature as a reference. It is noted that calibration curves for PSP-1 are independent of T and coalesce into a single line. On the other hand, calibration curves for PSP-2 and PSP-3 are temperature dependent. Table 2 shows Stern-Volmer coefficients, A and B, at 283.1K and 323.2K for each PSP. We define here the change in slope of the Stern-Volmer plot due to temperature variation as the following formula:

$$G = \frac{(B_2 - B_1)}{B_1} \cdot \frac{1}{DT} \cdot 100 \ [\%/\mathrm{K}], \tag{6}$$

Table 2. Stan-Volmer coefficients *A, B*

	T_1=283.1K		T_2=323.2K		Change in slope $(B_2-B_1)/B_1/(T_2-T_1)\times100$ %K
	A	$B(=B_1)$	A	$B(=B_2)$	
PSP-1	0.0548	0.9451	0.0233	0.9767	0.083
PSP-2	0.3019	0.6980	0.1510	0.8490	0.539
PSP-3	0.0920	0.9080	0.0436	0.9564	0.133

where, B_1 and B_2 are the Stern-Volmer coefficients B at 283.1K (reference) and 323.2K respectively, and DT (=40.1K) is temperature difference between the two cases. The change in slope for PSP-1, PSP-2 and PSP-3 is 0.083%/K, 0.539%/K and 0.133%/K respectively. Among the three PSPs, PSP-1 has the smallest change in slope with temperature. Furthermore, PSP-1 has the highest-pressure sensitivity among the three PSPs. The sensitivity of PSP-1 at T=283.1K is higher than that of PSP-2 and PSP-3 by 26% and 4% respectively.

Figure 4 compares temperature sensitivities of the three PSPs at P=100kPa. We define here the temperature sensitivity of PSP as a percent change in luminescent intensity per one degree at the reference condition. The temperature sensitivity for PSP-1, PSP-2 and PSP-3 at 100kPa and 283.1K is −1.3%/K, −2.0%/K and −2.2%/K respectively. It is noted here that there is considerable difference in the temperature sensitivity between PSP-1 (Poly-IBM-co-TFEM) and PSP-3 (poly-IBM). This illustrates that the fluorine group has the effect of increasing diffusivity of oxygen molecules in a paint layer and thus reducing the temperature sensitivity of the paint.

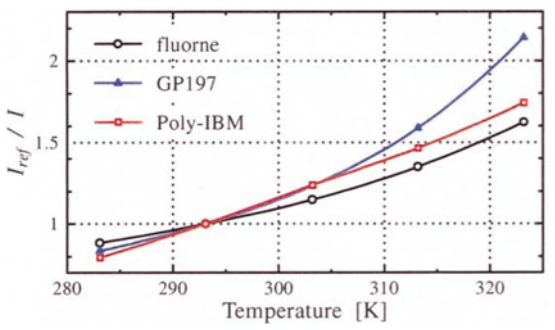

Fig. 4. Temperature dependency of luminescence intensity at P=100kPa for PSPs.

As a result of the calibration tests, PSP-1 was selected for use in wind tunnel tests of a delta wing model. The calibration result for PSP-1 was fitted to a linear line in the form of Eq. (4). The coefficients, A and B, were evaluated at several temperatures near the wind tunnel conditions. The values at intermediate temperatures were computed by linear interpolation.

4. Wind Tunnel Tests

4.1 Experimental Setup

Experiments were made in the 0.2-m Supersonic Wind Tunnel (SWT) at the National Aerospace Laboratory in Japan. The NAL 0.2-m SWT is a closed-circuit continuous wind tunnel driven by a multi-stage axial compressor. The test section is 0.2-m square and 0.4-m in length. The stagnation pressure, P_t, can be varied from 55kPa to 150kPa while the stagnation temperature is maintained around 333K.

Figure 5 shows a delta wing model used in this experiment. The model is made of aluminum and has a centerline chord, C, of 100mm. The leading edge is sharp with 70° sweep. The top surface of the model was coated with white optical undercoat first and then PSP was applied with an airbrush. Eight pressure taps were provided at the chordwise location of x/C=0.8 and the spanwise locations from S/S_{max}=0.2 to 0.9 at 0.1 steps. One thermocouple was soldered to the model support to monitor model surface temperature during tests. Measurements by PSP, pressure taps and a thermocouple, were made simultaneously. The model was strut-mounted in the center of the test section at attack angles of 20° and 30°.

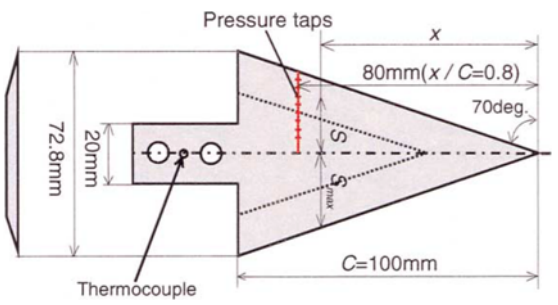

Fig. 5. Schematic of the deltawing model.

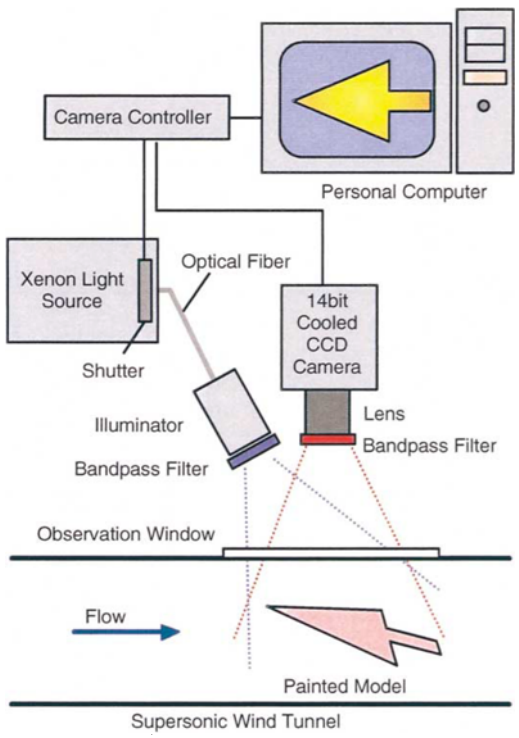

Fig. 6. Schematic sketch of the optical setup.

A schematic sketch of an optical setup for wind tunnel tests is shown in Fig. 6. To prevent systematic errors inherent to the measurement system, the same equipment (a light source, a CCD camera, filters and so on) was used in both calibration tests and wind tunnel tests. The wind-on images were recorded at each test condition after the model temperature was stabilized to reduce errors due to temperature dependency of PSP. The wind-off reference images were recorded soon after the tunnel was stopped so that the difference in model temperature between wind-on and off-wind conditions could be minimized. Twelve images were acquired for each test condition. The images obtained were then stored in a personal computer and analyzed after the tests to reconstruct pressure distribution maps.

4.2 Test Conditions

The test conditions for the 0.2-m SWT are tabulated in Table 3. Mach number M was varied from 0.58 to 0.78. At Mach number of 0.6, the stagnation pressure P_t was varied over the range from 55kPa to 100kPa with Reynolds number ($Re=UC/\nu$) from 5.67×10^5 to 9.97×10^5. It should be noted that the free-stream static pressure was measured with a static pressure tap located just upstream of the model support. Thus the presence of the model interfered with the static pressure measurement. In this experiment, no correction has been made for this interference so that pressure data was plotted in the dimensional form, not in the C_p form.

Table 3. Test conditions in the NAL 0.2m SWT.

Mach number M	Attack angle α degrees	Stagnation pressure P_t kPa	Reynolds number Re $\times10^5$
0.60–0.78	20	55	5.67–6.39
0.60	20	55–100	5.67–9.97
0.58, 0.78	30	30	6.1, 7.2

4.3 Data Reduction

The obtained images were reduced on a personal computer using Matlab software.

To cancel undesirable effects of uneven coating thickness and non-uniform illumination, it was necessary to take the ratio of wind-off and wind-on. In doing so, alignment or registration of the two images is dispensable to take account of the effects of modeldisplacement and deformation.

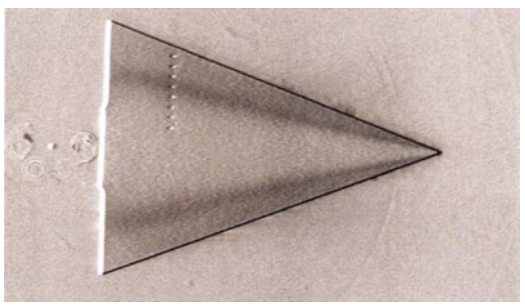

Fig. 7. Luminescent intensity ratio image without displacement correction.

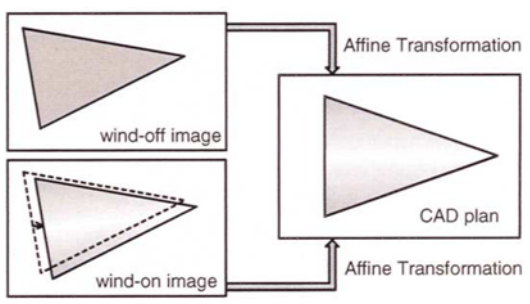

Fig. 8. Displacement correction by affine transformation.

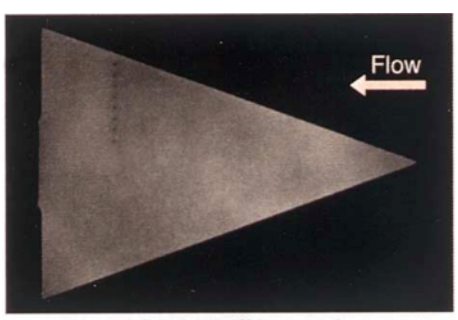

(a) Wind-off image I_{ref}

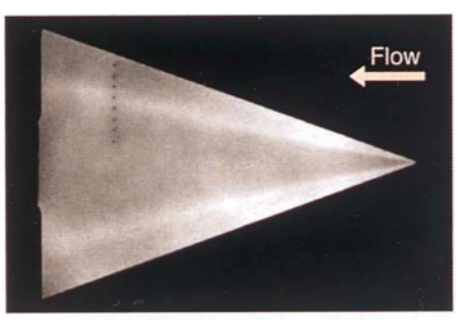

(b) Wind-on image I

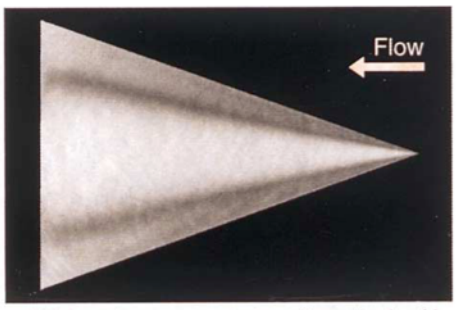

(c) Luminescence intensity ratio I_{ref} / I

Fig. 9. Processed images by image processing.

Figure 7 shows the luminescent intensity ratio image obtained with no correction for model displacement and deformation. It is clear that the model movement is a large source of error. To compensate for this, a CCD image of the delta wing was transferred to a physical plane by affine transformation as shown in Fig. 8. The affine transformation matrix, A, was computed from the following relationship.

$$A = \begin{pmatrix} x_1 & y_1 & 1 \\ x_2 & y_2 & 1 \\ x_3 & y_3 & 1 \end{pmatrix} \cdot \begin{pmatrix} a_1 & b_1 & 1 \\ a_2 & b_2 & 1 \\ a_3 & b_3 & 1 \end{pmatrix}^{-1} \tag{7}$$

where (a_n, b_n) $(n=1,2,3)$ are coordinates in the image plane of three apices of the delta wing model and (x_n, y_n) $(n=1,2,3)$ are coordinates in the physical plane (CAD geometry). Both wind-off and wind-on images are transformed to the physical plane using this transferring relation. It is easy to extract pressure values at any location because the measured pressure data are mapped onto the physical plane by this process. The sequence to convert luminescent intensity images to pressure distributions can be summarized as follows.

Process 1. Average several (four to twelve) images for each condition.

Process 2. Subtract a dark image from an averaged image to account for the camera dark current noise.

Process 3. Correct model displacement and deformation due to airflow.

Process 4. Apply spatial low-pass filter to the images.

Process 5. Take the ratio of wind-off and wind-on images to obtain reciprocal of luminescent intensity ratio, I/I_{ref}.

Process 6. Apply low-pass filter again to the luminescent intensity ratio image.

Process 7. Reconstruct pressure distribution from the luminescent intensity ratio image using static calibration data.

The shot noise of a CCD sensor can be reduced by an image averaging process (process 1). The signal to noise ratio changes in proportion to $1/\sqrt{2}$ to the number of averaged images.

As described above, an image of the delta wing was transferred to a physical plane by affine transformation to correct model displacement and deformation due to airflow (process 3). A spatial low-pass filter (processes 4 and 6) was applied to reduce high frequency noise in an image such as variation of pixel gain and heterogeneity of PSP coating. Shimbo et al. (1997, 1998) have applied a similar process to low-speed and transonic wind tunnel tests to reduce the spatial noise in PSP images.

Figures 9(a) and 9(b) show raw images at wind-off and wind-on conditions. The wind-on images were obtained at M=0.6, P_t=55kPa and a=20°. Figure 9(c) represents a processed image obtained through all the processes.

The effect of each process on reduced data is illustrated in Fig. 10. The data shown in Fig. 10 are the spanwise distribution of luminescent intensity ratio, I_{ref}/I, at x/C=0.5 for the same condition as in Fig. 9. Figures 10(a) and 10(b) show the results obtained without and with the registration procedure. It is seen that unrealistic pressure variation shown in Fig. 10(a) has been corrected in Fig. 10(b) by registration process.

The effect of image averaging is shown in Fig. 10(c). It is seen that the random noise such as shot noise of a CCD was reduced significantly. Low-pass filtering was also effective in reducing the spatial noise significantly as shown in Fig. 10 (d).

To convert the luminescent intensity ratio image into pressure distribution, we use the Stern-Volmer relation

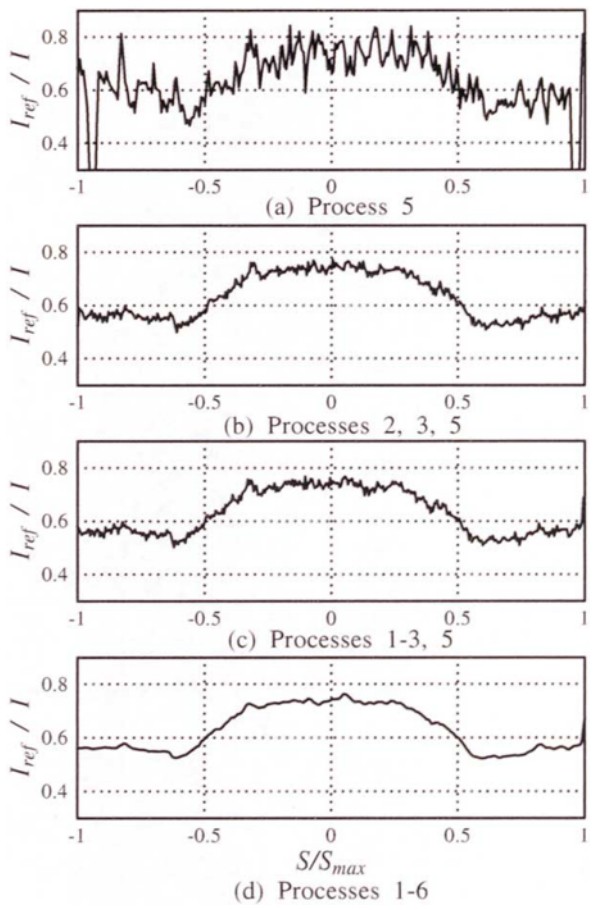

Fig. 10. Effect of image correction processes on reduced data at M=0.6, P_t=55kPa, a=20° and x/C=0.5.

obtained in a static calibration test. To take account of temperature difference between the wind-off and wind-on two images, Equation (4) is modified as

$$\frac{I(P_{ref},T_{ref})}{I(P,T)}=\frac{I(P_{ref},T_{ref})}{I(P_{ref},T)}\cdot\frac{I(P_{ref},T)}{I(P,T)}=\frac{I(P_{ref},T_{ref})}{I(P_{ref},T)}\cdot\left(A(T)+B(T)\cdot\left(\frac{P}{P_{ref}}\right)\right) \tag{8}$$

where P_{ref} and T_{ref} are known pressure and temperature at the reference wind-off condition. In this study, wind-off images taken after the wind tunnel test were used as a reference. The coefficients A and B were evaluated from the temperature measured using a thermocouple mounted on the model. It was verified by a separate test using temperature-sensitive paint that there was little variation in temperature on the model surface for both wind-off and wind-on cases. Thus, the pressure distribution map can be reconstructed from a luminescent intensity ratio image by using Eq. (8). This calibration method does not require any pressure tap data and is referred to as an a priori calibration.

4.4 Experimental Results

Figure 11 represents the pressure distributions obtained by PSP at the pressure tap location (x/C=0.8). Data for three test cases; (a) M=0.6, P_t=55kPa and α=20°, (b) M=0.78, P_t=55kPa and α=20°, and (c) M=0.6, P_t=90kPa and α=20° are shown. In Figs. 11(a) and 11(b), the PSP-derived data are in good agreement with the pressure tap data. The maximum differences in pressure are 1.2kPa and 1.6kPa for cases (a) and (b) respectively, which corresponds to about 2.2% and 2.9% of the stagnation pressure. On the other hand, the maximum pressure difference for case (c) is as much as 3.7kPa, which is 4.1% of stagnation pressure. This is resulting from the fact that camera exposure time was kept constant for all cases so that the signal to noise ratio became worse as the luminescent intensity decreased with increasing pressure.

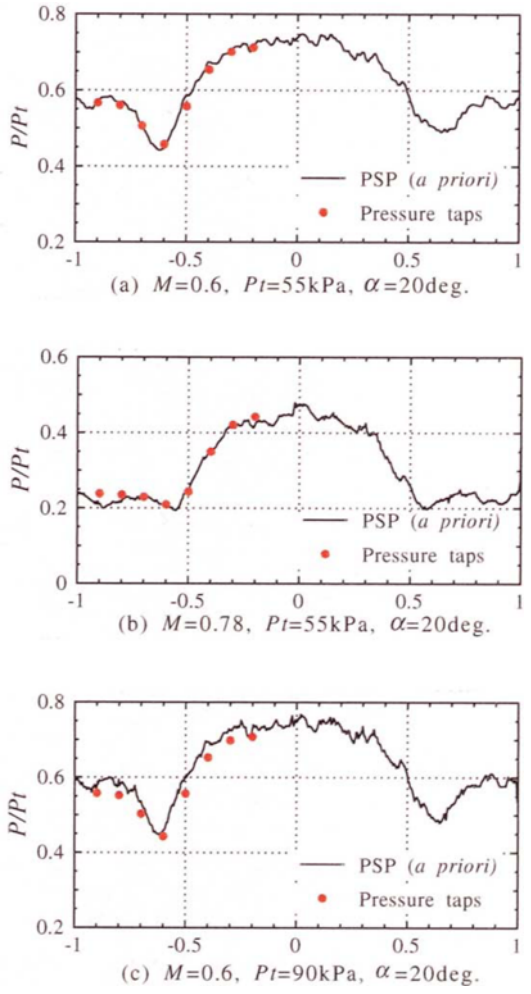

Fig. 11. Comparison between PSP (*a priori*) and pressure tap data along the pressure tap rows at x/C=0.8.

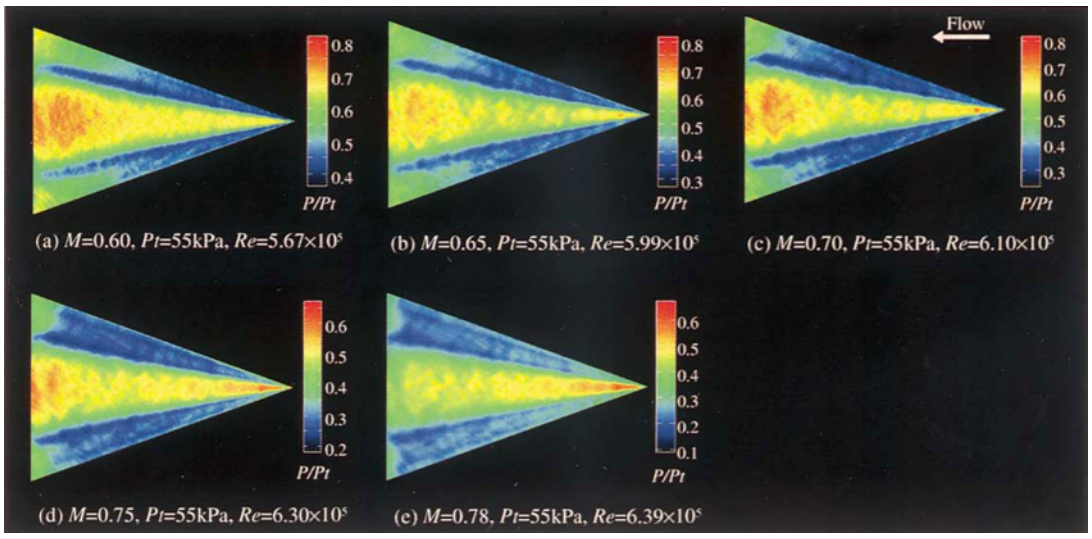

Fig. 12. Mach number effect for M=0.6 through 0.78, P_t=55kPa and a=20°.

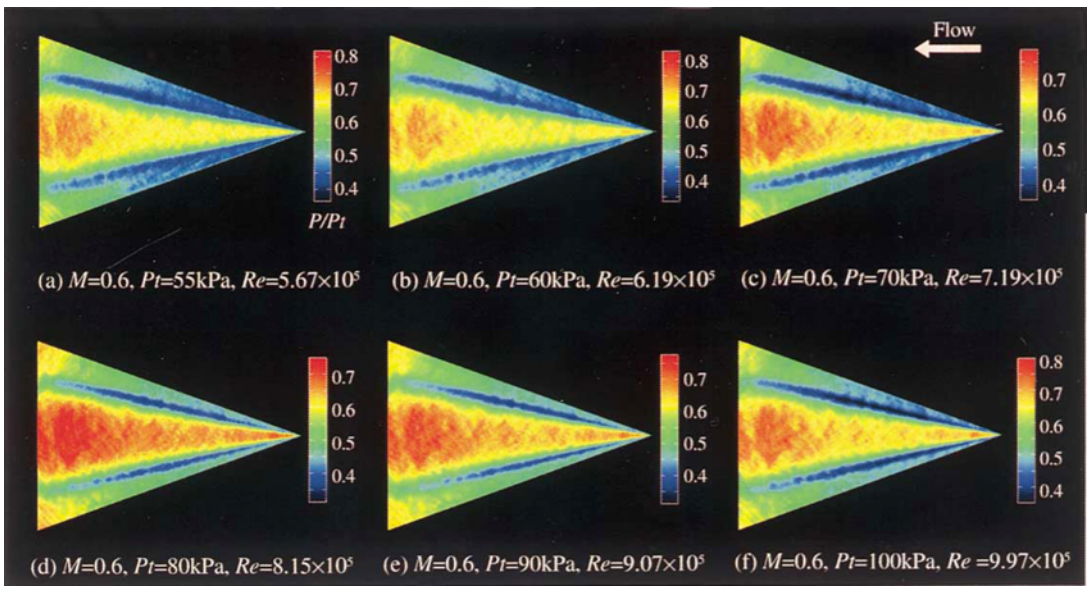

Fig. 13. Reynolds number effect for Re=5.67×10^5 to 9.97×10^5, M=0.6 and a=20°.

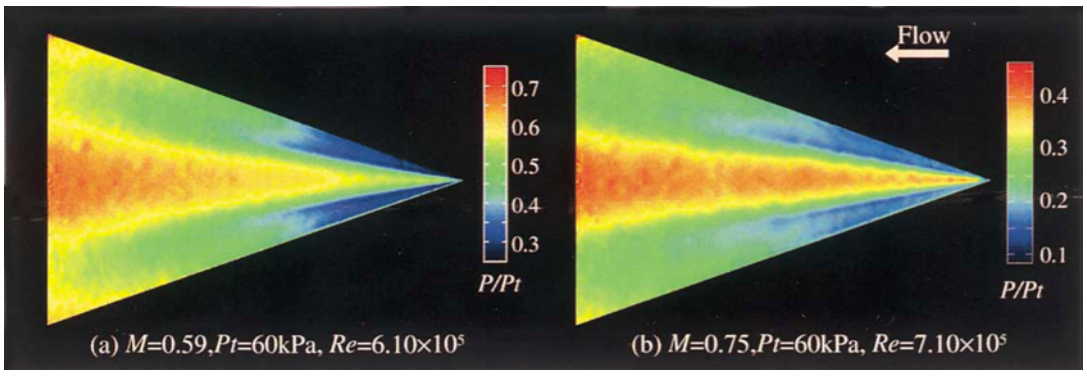

Fig. 14. Pressure distribution map at a=30°, M=0.59 and 0.75 and P_t=60kPa.

Figure 12 shows the effect of Mach number on pressure distribution on the delta wing. The Mach number was varied from M=0.6 to 0.78 with P_t and a kept constant at 55kPa and 20° respectively. It is seen that a complicated flow field including primary and secondary leading-edge separation vortices rolled up from the leading edges has been clearly visualized. At M=0.6, the primary vortices keep their structures until they reach the trailing edge while the secondary vortices (shown between the leading-edge and primary vortices) are broken down at the axial location around x/C=0.5. At M=0.78 (Fig. 12(d)), both the primary and secondary vortices are not broken down on the model. As Mach number increases, the location of secondary vortex breakdown moves downstream and the high-pressure region near the wing centerline spreads over the apex. This is attributed to the fact that the primary vortices get stronger with increasing Mach number.

Figure 13 shows the effects of Reynolds number on the pressure distribution for M=0.6 and a=20°. Reynolds number was varied from Re=5.67×10^5 to 9.97×10^5 by changing stagnation pressure. Although the Reynolds number has been changed by a factor of 1.8, the basic flow structure looks almost unchanged. This indicates that, at this condition, the change in Reynolds number has little influence on the vortex formation. Elsenaar et al. (1988) suggested that Reynolds number would be less important for the sharp leading-edge. Our observation has confirmed this statement.

Figure 14 shows the result for a=30°. The breakdown of vortices occurrs earlier at a=30° than at a=20°(Fig. 12). At M=0.59, the primary vortices were broken down at x/C=0.45. It is seen that the low-pressure region is located near the apex and along the leading edge. It is interesting that the high-pressure region in the model centerline is spread over the trading edge. At M=0.75, the vortex breakdown occurs around x/C=0.7. The location of vortex breakdown moves downstream with increasing Mach number. This is similar to the result for a=20°.

5. Conclusions

1) PSP with new fluoropolymer binder shows higher-pressure sensitivity and lower-temperature sensitivity than conventional PSP with silicone polymer. This PSP can reduce a pressure measurement error due to temperature variation during the test.
2) A delta wing model was tested using PSP with fluoropolymer binder. An *a priori* calibration was applied to reconstruct pressure distribution from the luminescent intensity ratio image. The PSP-derived data show good agreement with pressure tap data. The absolute error is about 1.6kPa for P_t =55kPa test cases.
3) The complicated flow field on the delta wing was clearly visualized by PSP, including primary and secondary vortices and their breakdown. It was observed that an increase of Mach number had the effect of delaying vortex breakdown while the change in Reynolds number had little influence on breakdown for the sharp-edged delta wing.
4) This experiment has demonstrated that PSP is a versatile tool for quantitatively visualizing pressure distributions over the model surface. PSP is useful not only in studying the basic phenomena of fluid dynamics but also in designing aircraft and other flying vehicles.

References

Amao, Y., Asai, K., Miyasita, T. and Okura, I., Photophysical and Photochemical Properties of Optical Oxygen Pressure Sensor of Platinum Porphyrin-Isobutylmethacrylate-Trifluoroethylmethacrylate Copolymer Film, Polymer Journal, 31-12 (1999), 1267-1296.

Elsenaar, A., Hjelmberg, L. and Buetefisch, K., The International Vortex Flow Experiment, AGARD CP-437, Paper 9, (1988).

Liu, T., Guille, M. and Sullivan, J. P., Uncertainty Analysis of Pressure Sensitive Paint Measurement, AIAA Paper 99-3785 (1999).

Liu, T., Campbell, B. T., Burns, S. P. and Sullivan, J. P., Temperature and Pressure-Sensitive Luminescent Paints in Aerodynamics, Apl. Mech. Rev., 50-4 (1997), 227-246.

Shimbo, Y., Mehta, D. R. and Cantwell, J. B., Vortical Flow Field Investigation Using the Pressure Sensitive Paint Technique at Low Speed, AIAA Paper 97-0388 (1997).

Shimbo, Y., Asai, K., Kanda, H., Iijima, I., Komatu, N., Kita, S. and Ishiguro, M., Evaluation of Several Calibration Techniques for Pressure Sensitive Paint in Transonic Testing, AIAA Paper 98-2502 (1998).

Author Profile

Yasuhiro Egami: He received his B.Sc. (Eng.) degree in 1992 and Doctor degree of Engineering in 1997 in Tohoku University in Japan. He worked as a research associate at Institute of Fluid Science, Tohoku University from 1997 to 1999. He worked as an invited researcher at Karlsruhe University during 1998-1999. He started to work as a research fellow at National Aerospace Laboratory since 1999. His current research interest is to develop PSP and TSP technique and their application to fluid dynamics testing.

Yoshimi Iijima: He received the B.E. degree in Electrical Engineering from Science University of Tokyo in 1997. He has been working at National Aerospace Laboratory since 1992. His current research interest is to develop PSP and TSP technique and their application to fluid dynamics testing.

Yutaka Amao: He received Doctor degree of Engineering in 1997 in Tokyo Institute of Technology in Japan. He worked as a researcher at Kanagawa Academy of Science and Technology from 1997 to 1998. He started to work as a research fellow at National Aerospace Laboratory since 1998. His current research interest is to develop optical sensor technique using photofunctional materials.

Keisuke Asai: He graduated from Kyoto University in 1980 (Bachelor of Aeronautical Engineering) and received PhD (Aerospace Engineering) from The University of Tokyo in 1995. He has been working as a research scientist at National Aerospace Laboratory since 1980. His current position is group leader of Advance Measurement Technology Group in Fluid Science Research Center. He also serves as project manager of MOSAIC, an interdisciplinary R&D project to develop molecular sensor technology for aero-thermodynamic research. He is Associate Fellow of AIAA, Member of JSASS and Visualization Society of Japan.

Akihiko Fuji: He graduated from The Tokyo University of Agriculture and Technology, and received the B.Sc. (Eng.) degree in 2000. He is a master course student of the same University. The objective of his present study is fatigue analysis of rolling bearing.

Norikazu Teduka : He graduated from The Tokyo University of Agriculture and Technology, and received the B.Sc. (Eng.) degree in 1999. He is a master course student of the same University. The objective of his study is time response of PSPs for using in unsteady pressure measurements.

Masaharu Kameda: He received his B.S., M.S. and Ph.D. degrees in Mechanical Engineering from The University of Tokyo in 1989, 1991 and 1994, respectively. After he received his Ph.D. degree, he has been affiliated with the Department of Mechanical Systems Engineering at The Tokyo University of Agriculture and Technology (TUAT), where he is now an associate professor. His research has been in the field of bubble dynamics, nonlinear acoustics, aerodynamics and flow visualization.